

Northumbria Research Link

Citation: Adams, Natalie E., Teige, Catarina, Mollo, Giovanna, Karapanagiotidis, Theodoros, Cornelissen, Piers, Smallwood, Jonathan, Traub, Roger D., Jefferies, Elizabeth and Whittington, Miles A. (2019) Theta/delta coupling across cortical laminae contributes to semantic cognition. *Journal of Neurophysiology*, 121 (4). pp. 1150-1161. ISSN 0022-3077

Published by: American Physiological Society

URL: <https://doi.org/10.1152/jn.00686.2018> <<https://doi.org/10.1152/jn.00686.2018>>

This version was downloaded from Northumbria Research Link:
<http://nrl.northumbria.ac.uk/id/eprint/37843/>

Northumbria University has developed Northumbria Research Link (NRL) to enable users to access the University's research output. Copyright © and moral rights for items on NRL are retained by the individual author(s) and/or other copyright owners. Single copies of full items can be reproduced, displayed or performed, and given to third parties in any format or medium for personal research or study, educational, or not-for-profit purposes without prior permission or charge, provided the authors, title and full bibliographic details are given, as well as a hyperlink and/or URL to the original metadata page. The content must not be changed in any way. Full items must not be sold commercially in any format or medium without formal permission of the copyright holder. The full policy is available online: <http://nrl.northumbria.ac.uk/policies.html>

This document may differ from the final, published version of the research and has been made available online in accordance with publisher policies. To read and/or cite from the published version of the research, please visit the publisher's website (a subscription may be required.)

1
2 **Theta/delta coupling across cortical laminae**
3 **contributes to semantic cognition.**

4
5 **Short title: Theta/delta interactions in semantic processing**

6
7 Natalie E Adams¹, Catarina Teige², Giovanna Mollo², Theodoros Karapanagiotidis², Piers L
8 Cornelissen³, Jonathan Smallwood², Roger D Traub⁴, Elizabeth Jefferies², Miles A Whittington*¹

9
10
11 1. HYMS, University of York, YO10 5DD, UK

12 2. Dept. Psychology, University of York, YO10 5DD.

13 3. Dept Psychology, School of Life Sciences, Northumbria University, Newcastle upon Tyne, NE1 8ST
14 UK

15 4. AI Foundations, IBM T.J. Watson Research Center, Yorktown Heights, NY 10598, USA.

16
17 *Corresponding author:*

18 Miles Whittington

19 Hull-York Medical School

20 University of York

21 YO10 5DD

22 Tel: 01904 328755

23 Email: miles.whittington@hyms.ac.uk

24
25 **Running head:** Cross frequency coupling in semantic cognition.

26
27
28
29
30
31

32

33 **Abstract**

34 Rhythmic activity in populations of neurons is associated with cognitive and motor function. Our
35 understanding of the neuronal mechanisms underlying these core brain functions has benefitted
36 from demonstrations of cellular, synaptic and network phenomena leading to the generation of
37 discrete rhythms at the local network level. However, discrete frequencies of rhythmic activity rarely
38 occur alone. Despite this, little is known about why multiple rhythms are generated together or what
39 mechanisms underlie their interaction to promote brain function. One overarching theory is that
40 different temporal scales of rhythmic activity correspond to communication between brain regions
41 separated by different spatial scales. To test this we quantified the cross-frequency interactions
42 between two dominant rhythms – theta and delta activity - manifest during MEG recordings of
43 subjects performing a word-pair semantic decision task. Semantic processing has been suggested to
44 involve the formation of functional links between anatomically disparate neuronal populations over
45 a range of spatial scales and a distributed network was manifest in the profile of theta-delta coupling
46 seen. Furthermore, differences in the pattern of theta-delta coupling significantly correlated with
47 semantic outcome. Using an established experimental model of concurrent delta and theta rhythms
48 in neocortex we show that these outcome-dependent dynamics could be reproduced in a manner
49 determined by the strength of cholinergic neuromodulation. Theta-delta coupling correlated with
50 discrete neuronal activity motifs segregated by cortical layer, neuronal intrinsic properties and long-
51 range axonal targets. Thus, the model suggested that local, interlaminar neocortical theta-delta
52 coupling may serve to coordinate both cortico-cortical and cortico-subcortical computations during
53 distributed network activity.

54

55 **Keywords**

56 Cross frequency coupling, semantic processing, delta rhythm, theta rhythm

57

58 **New and Noteworthy**

59 Here we show, for the first time, that a network of spatially distributed brain regions can be revealed
60 by cross-frequency coupling between delta and theta frequencies in subjects using MEG recording
61 during a semantic decision task. A biological model of this cross-frequency coupling suggested an

62 interlaminar, cell-specific division of labour within neocortex may serve to route cortico-cortical and
63 cortico-subcortical information flow to promote such spatially distributed, functional networks.

64 **Introduction**

65 Rhythmic electrical activity in discrete frequency bands accompanies a broad range of motor,
66 affective and cognitive processes in the brain. Evidence for a direct, causal role in cognitive
67 processing has been postulated for some time (e.g. Basar et al., 2001), with different frequencies
68 involved to different extents in different tasks. For example, gamma rhythms organise primary
69 sensory information to facilitate higher-order processing (Fries, 2015); beta rhythm generation
70 correlates with task performance requiring short-term memory and prediction (Arnal & Giraud,
71 2012); alpha rhythms control access to stored memories (Klimesch, 2012); theta rhythms appear to
72 be required for sequential processing of sensory information (Remondes & Wilson, 2013); delta
73 rhythms appear vital for semantic processing (Harmony, 2013). Where the information is available,
74 these rhythms appear to have an origin in subsets of neurons in local cortical and thalamic circuits
75 (Roopun et al., 2008), but the temporal organisation they impart onto local circuit outputs is vital for
76 control of information flow within the wider cortical mantle (e.g. Akam & Kullmann, 2010; Li et al.,
77 2017).

78 Having a large library of rhythms available to local cortical circuits makes for a complex temporal
79 landscape. However, the situation is further complicated by observations showing that discrete
80 rhythms are rarely generated alone. Coexistence of multiple frequencies of activity, each temporally
81 interacting with one another, is a common feature of brain dynamics (Lakatos et al., 2005) but we
82 understand little about the mechanisms that facilitate these interactions, nor the computational
83 advantages they may impart: Do they just represent a simple additive process, with one brain region
84 involved simultaneously in multiple cortical processes, or is there synergy at work, with the presence
85 of multiple, interacting rhythms superadditive for cortical function? There is increasing evidence for
86 the latter, leading to the current working hypothesis that different frequencies of rhythm chaperone
87 cortical communication on different spatial scales (Kopell et al., 2000; Canolty & Knight, 2010).

88 To address this issue we use a semantic cognition task to quantify changes in the outcome-
89 dependent pattern of interaction between the two cardinal rhythms involved (theta and delta
90 frequency activity). Semantic cognition assigns meaning to the stream of sensory inputs we
91 experience during wakefulness (Corbett et al., 2009) and has been shown to involve interaction
92 between many brain regions on multiple spatial scales (Binder et al., 2009). Functional neuroimaging
93 studies suggest a 'hub and spoke'-like structure to semantic representation networks (Patterson et

94 al., 2007). Activity locally seen within hub regions (e.g. Mollo et al., 2017) provides amodal rendering
95 of semantic information (e.g. anterior temporal lobe, ATL) and comparators to prior schema leading
96 to appropriate behavioural responses (e.g. posterior middle temporal gyrus, intraparietal sulcus;
97 pMTG, IPS). This local activity needs to be distributed over broader spatial scales for appropriate
98 semantic cognition to take place. Interaction between the above hub regions and language centers
99 (LIFG, Sharot et al., 2012), executive control regions (Duncan, 2010) and parietal areas involved in
100 polymodal sensory integration, attention and spatial cognition is also required (AG, Binder et al.,
101 2009).

102 Flow of information between different regions involved in the semantic network most likely depends
103 upon theta and delta frequency temporal patterns. Evidence for a role for theta-alpha rhythms (5-12
104 Hz) in semantic processing has been seen both in general in cortex (Klimesch et al., 1994) and
105 specifically in ATL (van Ackeren & Rueschemeyer, 2014). Indirect evidence also suggests an
106 involvement of activity at delta frequency: The N400 component of event related potentials –
107 thought to represent a phase-resetting of on-going delta rhythms (van Petten & Luka, 2006) – is a
108 marker for semantic cognition (Koelsch et al., 2004) and communication between frontal and
109 parietal regions of semantic relevance is mediated by delta rhythms (1-4 Hz) during decision tasks
110 (Nacher et al., 2013). The decision-making component of semantic processing also suggests
111 importance for theta and delta rhythms: Activity across the theta-delta bands (2-9 Hz) relates to
112 models of activity in which neurons coding for a particular outcome receive increasing levels of
113 excitation over time (i.e. a ‘ramp’ of synaptic input) (Wang, 2002; Purcell et al., 2010; Hunt et al.,
114 2012). In addition, iterative switching between discrete neuronal activity states at approximately
115 theta frequency correlates with decision-making in frontal regions (Rich & Wallis, 2016).

116 Given these proposed roles for theta and delta frequency activity in semantic cognition we then use
117 a local circuit, biological model of these rhythms (Carracedo et al., 2013) to identify possible *cellular*
118 origins for their pattern of interaction. The profile of theta/delta interaction changes during the
119 semantic task could be accurately reproduced in this local circuit model. The known connectivity
120 properties of the cellular substrates identified by the model support the ‘different rhythms –
121 different spatial scales’ hypothesis (Canolty & Knight, 2010) and suggest further refinement:
122 Different frequencies of rhythm interact to coordinate cortico-cortical and cortico-subcortical
123 functional connectivity.

124

125 **Methods**

126 *Participants.*

127 17 healthy, female, right-handed native English speakers (mean age 23.3 years, age range 20–35
128 years) with normal or corrected-to-normal vision participated in this study under written consent
129 and following ethical approval (York Neuroimaging Centre, University of York).

130 *Task.*

131 The task is shown schematically in Fig 2a. Stimuli were adapted from Badre et al (2005) and involved
132 sequential visual presentation of word pairs with varying levels of association. Subjects were
133 requested to consider whether the word pairs were semantically related. Subjects were not aware of
134 this aspect of the task structure. Related word combinations were selected using the Edinburgh
135 Associative Thesaurus to identify words that were produced frequently together by 22% of
136 participants. Unrelated word combinations were created by shuffling these data sets and removing
137 coincidentally related pairs. The words were all nouns with a concreteness rating >500 as specified in
138 the MRC psycholinguistic database (Wilson, 1988). Each word appeared once in both the related and
139 unrelated conditions. Red fixation lines were always present on the screen, with words shown in
140 light grey on a dark grey background (as in Fig 2a). The screen was positioned 75 cm from the viewer
141 and the image projected in a way that words subtended 1 degree vertically and 5 degrees
142 horizontally at the retina. First word presentation occurred 800 ms into the task for a duration of
143 200 ms. The second word presentation occurred at 1150 ms, again for 200 ms. The trial length was
144 3550 ms with a jitter of between 0 – 1000 ms between adjacent trials. 10% of trials were catch trials
145 where participants were cued via a question mark on the screen to press a button to indicate
146 whether the words in the pair were related. These trials were used to monitor reaction time (RT)
147 performance and the behavioural response of interest: semantic decision ('related' vs. 'unrelated')
148 for each subject/word pair. The catch trial and following trial were excluded from further analyses to
149 avoid contamination from motor artefacts.

150 *Data acquisition.*

151 High resolution T1-weighted MR structural scans (method adapted from Kozinska et al., 2001) were
152 acquired on a GE 3.0T Signa Excite HDX with an image resolution of 1.13mm and used for MEG co-
153 registration. MEG data was acquired using a 4D Neuroimaging Magnes 3600 Whole Head 248
154 Channel SQUID Magnetometer based system. Co-registration was achieved with a Polhemus Fastrak
155 (Colchester, VT 05446, USA) and 5 fiducial coils allowed for movement tracking. Data was acquired in
156 a dark, magnetically isolated room and at a sample rate of 678.17 Hz (low-pass filtered to 200 Hz).
157 Raw MEG data is available on request from beth.jefferies@york.ac.uk.

158 *Virtual electrodes.*

159 "Virtual electrodes" were constructed using a Linearly Constrained Minimum Variance beamformer
160 using the technique described by van Veen (1997). The spatial filters were constructed using a
161 covariance matrix calculated from all of the data and a multiple-spheres forward model (Huang
162 1999). Following co-registration with each subject's structural MRI scan coordinates were specified
163 in standard MNI space, with individual coordinate spaces transformed to standard space. The first
164 PCA component of the three orientations was used to create timeseries data. The extraction of
165 beamformed data, and the analyses below, were performed using the York Neuroimaging Analysis
166 Framework (publicly available at <http://vcs.ynic.york.ac.uk/docs/naf/index.html>) and standard
167 Matlab signal processing routines.

168 *Selection of regions of interest.*

169 A 3D lattice of points was constructed across the whole brain with 5 mm spacing, and beamformers
170 (above) were used to compute the total power at each point using the Neural Activity Index (NAI)
171 (van Veen, 1997). This approach was used to assess any changes in magnitude of the two
172 frequencies of interest (theta and delta rhythms, Fig 3b). However, owing to combinatorial issues
173 and computational demand, more detailed spatiotemporal analyses were performed on a much
174 smaller number of sites chosen for their precedented involvement – in terms of task- and state-
175 dependent significant fMRI activations - in visual primary sensory (Banko et al., 2011) and semantic
176 processing (eg. Visser et al., 2010). Regions involved in control, default, memory and network
177 switching tasks (eg. Christoff et al., 2009) were also included for comparison.

178 Chosen coordinates for left (L) and right (R) hemispheres were as follows (numbered in bold
179 according to the matrices shown in Fig. 2): **1**) medial frontal gyrus (LMFG: -27, 23, 48); **2**) angular
180 gyrus (LAG: -41, -60, 29); **3**) posterior medial temporal gyrus (LpMTG: -64, -20, -9); **4**) posterior
181 cingulate cortex (LPCC: -7, -52, 26); **5**) dorso-medial prefrontal cortex (LdMPFC: -7, 49, 18); **6**) ventro-
182 medial prefrontal cortex (LvMPFC: -6, 52, -2); **7**) anterior temporal lobe superior temporal gyrus
183 (LATL_aSTG: -57, 6, -18); **8**) anterior insular cortex (LAIC: -30, 18, 4); **9**) posterior insular cortex (LPIC:
184 -36, 4, -2); **10**) inferior parietal sulcus (LIPS: -43, -50, 46); **11**) posterior inferior frontal gyrus (LpIFG: -
185 47, 21, 18); **12**) left hippocampus (LHIPP: -25, -32, -18); **13**) left primary visual cortex (LV1: -15, -96,
186 6); **14**) medial frontal gyrus (RMFG: -27, 23, 48); **15**) right angular gyrus (RAG: 41, -53, 26); **16**) right
187 posterior mid-temporal gyrus (RpMTG: 64, -20, -9); **17**) right posterior cingulate cortex (RPCC: 7, -46,
188 26); **18**) right dorsomedial prefrontal cortex (RdMPFC: 7, 49, 18); **19**) right ventromedial prefrontal
189 cortex (RvMPFC: 10, 50, 0); **20**) right anterior temporal lobe/superior temporal gyrus (RATL_aSTG:

190 57, 9, -18); **21**) right anterior insular cortex (RAIC: 34, 16, 4); **22**) right posterior insular cortex (RPIC:
191 38, 5, -2); **23**) right inferior parietal sulcus (RIPS: 52, -60, 44); **24**) right posterior inferior frontal gyrus
192 (RpIFG: 47, 18, 18); **25**) right hippocampus (RHIPP: 32, -40, -16); **26**) right primary visual cortex (RV1:
193 15, -96, 6).

194 *Analysis.*

195 *Pre-processing:* For each trial/subject, beamformed channels containing movement artefacts, eye
196 blinks and external noise were excluded leaving 70-130 trials for each condition (related or
197 unrelated word pairs) for each subject. Data epochs for each trial (length 3350 ms, see 'task' above)
198 were then filtered from 0.5-45 Hz using a zero-phase, finite impulse response filter (Matlab) to
199 preserve both phase information and the original sample rate (678.17 Hz) for analysis of temporal
200 structure. For analyses focussing on theta and delta rhythms we first identified the subject mean
201 modal peak frequencies in the timeseries data epochs from 1st stimulus presentation to RT. These
202 were 5.2 Hz (used as the theta frequency reference) and 2.5 Hz (delta frequency) (see Fig. 3a). For
203 theta/delta phase-amplitude coupling analyses band-pass filtered timeseries were generated from
204 4.5-7.5 Hz and 1.0 – 4.0 Hz.

205 *Region activation:* Changes in event-related potentials (ERPs), particularly the N400 component,
206 have been linked to semantic processing previously (Koelsch et al., 2004). We therefore quantified
207 stimulus-induced deviations from baseline (the first 800 ms of each trial prior to presentation of the
208 1st stimulus) as magnitude changes above threshold in the virtual electrode data. Threshold was
209 defined by analysing the distribution for all virtual electrode activity for each subject and set at two
210 standard deviations above the baseline mean (i.e. above the 5% significance level, Fig. 1a). This
211 method captured both the initial ERP and any subsequent, significant deviations leading up to the
212 decision time (i.e. 800 ms – RT for each trial/subject. Regions shown to be active during the task in
213 general (at any time from presentation of 1st stimulus to RT) were then subdivided according to each
214 subject's semantic decision ('related' or 'unrelated') on a trial-by-trial basis.

215 *Temporal cross-covariances:* Two measures of pairwise temporal relationships between virtual
216 electrode activity were used on the data epoch between 1st stimulus presentation to RT. Firstly,
217 synchrony is recognised as a key mechanism used by the cortex to code for properties of sensory
218 stimuli (Gray et al., 1989). We calculated pairwise synchrony as the mean magnitude of the
219 crosscovariogram around 0 ms (-25ms to +25 ms) lag for each pair of electrodes (Fig 1b) using the
220 signal processing toolbox in Matlab. Data were Hamming windowed with window length of 300 ms
221 and overlap of 285 ms. Secondly, covariance between electrode pairs at theta frequency –

222 particularly with half a theta cycle temporal separation – has been demonstrated as a signature of
223 functional connectivity between brain regions (Mizuseki et al., 2009). We therefore took the
224 magnitudes of the pairwise crosscovariogram around +96 ms and -96 ms (192 ms = 5.2Hz – the mean
225 theta frequency for this subject cohort). These were meaned between 25 ms either-side of these
226 phase values. Pairwise synchrony and theta covariance thresholds were again set at 2 standard
227 deviations over the mean crosscovariance data distribution.

228 *Phase-amplitude coupling (PAC):* More complex temporal signatures, particularly cross-frequency
229 coupling, are known to play an important role in long-range network function during cognition
230 (Canolty & Knight, 2010). We therefore focussed on interactions between the two dominant
231 frequencies expressed between stimulus presentation and RT: Delta-theta coupling was quantified
232 using the method described in Kramer & Eden (2013) using meaned traces from each region node
233 for each subject. Electrode data was band-pass filtered to extract activity in the delta band and theta
234 band based on the cohort mean delta and theta frequencies (e.g. see above and Fig. 3a). The
235 absolute component of the Hilbert transform of the theta channel was plotted relative to the phase
236 of each delta period between stimulus presentation and response time (2-5 delta periods per
237 subject/electrode). This method exposed any changes in theta rhythm magnitude relative to the
238 concurrent delta rhythm phase (Fig.1c). Analysis data is presented on a linear plot to demonstrate
239 any changes in the PAC profile for each task outcome. A false-detection-rate analysis (Storey &
240 Tibshirani, 2003) was then performed to extract any statistical differences from shuffled theta
241 channel data ($P > 0.05$) and the significant PAC scores displayed on polar plots (e.g. Figs. 4 & 7). Raw
242 data for this analysis was selected to meet the criteria suggested by Aru et al., 2015 for cross-
243 frequency analysis in all aspects except ‘input-related non-stationarities’ – phase reset could not be
244 discounted as it is a fundamental property of the delta and theta rhythms and vital for their role in
245 cognition (Cobb et al., 1995; Calderone et al., 2014, see discussion).

246

247 *In vitro model:* Cognitively-relevant phenomena in human EEG, MEG and fMRI datasets are often
248 modelled to suggest underlying network mechanisms. Neural, computational and statistical models
249 have been applied to semantic cognition (Ralph et al., 2017) but rarely inform with sufficient
250 objectivity and biological detail to suggest cell- and local network-level mechanisms. This is
251 particularly pertinent when considering the origin of brain dynamic signatures of cognitive relevance
252 for two reasons: Firstly, the minimum network substrates underlying known mechanisms of brain
253 rhythms are all, to date, contained in local circuits anatomically smaller than the maximum spatial
254 and/or temporal resolution of non-invasive techniques; Secondly, the different neuronal subtypes

255 involved in generation of different rhythms have different anatomical projection profiles which limit
256 – and thus point towards - their possible involvement in communication across multiple, distributed
257 regions (see discussion). Coupled delta and theta rhythms have been modelled at the local circuit
258 level previously in rodent association cortical regions anatomically corresponding to areas known to
259 be involved in human semantic cognition (Carracedo et al., 2013). In this model the two coexistent
260 rhythms were generated locally by subnetworks involving neurons with very different long-range
261 projection profiles: Regular spiking neurons (RS, theta) projecting purely cortico-cortically and
262 intrinsic bursting neurons (IB, delta) projecting subcortically (Groh et al., 2010; Kim et al., 2015). We
263 therefore used this model to identify possible neuronal substrates for semantic decision-related
264 changes in theta/delta coupling in local circuits. We then related model data to the ‘different
265 frequencies – different spatial scales’ hypothesis.

266 Briefly, horizontal and thalamocortically-oriented slices (450 μm thick) containing parietal cortex
267 were taken from male Wistar rats (150-300g) according to the UK Home Office Animals (Scientific
268 Procedures) Act 1986. Slices were transferred to an interface chamber and perfused with
269 oxygenated artificial cerebrospinal fluid (aCSF) (in mM: 126 NaCl, 3 KCl, 1.25 NaH_2PO_4 , 0.6mM
270 MgSO_4 , 1.2 CaCl_2 , 24 NaHCO_3 and 10 glucose) at 32 °C. Delta rhythms occurred spontaneously and
271 persistently in the presence of 2-6 μM carbachol – an analogue of acetylcholine. Extracellular field
272 recordings were performed with aCSF-filled glass micropipettes (2-5 $\text{M}\Omega$) and were bandpass filtered
273 at 0.1Hz to 300Hz to provide a local reference for the neocortically generated delta rhythm.
274 Intracellular recordings were performed with 2M potassium acetate-filled glass micropipettes (50-
275 150 $\text{M}\Omega$) and were low-pass filtered to 2.5kHz. Neuron subtypes were quantified by response to
276 depolarising current step (0.2 nA, 200 ms) from resting membrane potential. Statistical analysis of
277 excitatory synaptic inputs (EPSPs) and action potential (AP) outputs was performed with a repeat
278 measures ANOVA to examine the effects of experimental condition (different concentrations of
279 carbachol) over delta phase. Significant (using FDR test) coupling between the field delta rhythm and
280 EPSP/AP profiles are displayed in polar plots (Fig. 7).

281

282 **Results**

283 *Basic ERP electrophysiology revealed sensory task-dependent but not semantic interpretation-*
284 *dependent brain regions.* No significant differences in behavioural performance were seen between
285 each semantic interpretation ($P < 0.05$, Fig. 2a,b). Similarly, the magnitude of the suprathreshold
286 event related potential (ERP) changes also showed no correlation with behavioural performance. A

287 spatiotemporal sequence of regional activations was seen for each subject distributed around the
288 time of second stimulus presentation (Fig. 2ci). However, while no set of regions active at any time
289 between stimulus presentation and RT was common to all subjects when analysed by semantic
290 outcome (word-pairs seen as related or unrelated), a set of regions showed activation ($>2SD$ above
291 baseline) in response to task in general in all subjects (Fig. 2cii). These regions were all posterior and
292 consisted of bilateral primary visual, posterior cingulate and parietal areas along with both
293 hippocampi, though measurement from this deep-lying structure with non-invasive methods is
294 notoriously unreliable (Fig. 2ciii). No involvement of the frontal or temporal semantic regions used
295 for analysis was exposed using this basic measure of local activity. Thus, region activation alone
296 failed to capture the semantic decision-making process.

297 *Theta/delta spectral content dominated the epoch between stimulus presentation and response but*
298 *did not associate with semantic interpretation.* The above data demonstrated that different semantic
299 decision outcomes did not associate with magnitude changes in ERP in the individual regions
300 analysed here. However, data also showed dominant, spectrally discrete delta and theta frequency
301 peaks during the time from stimulus presentation to behavioural response (Fig. 3ai,ii). Band-pass
302 filtering of these delta (1-4 Hz) and theta (4.5-7.5 Hz) components revealed no significant global
303 differences in power in the time-period from presentation of the stimuli to a 'related' and
304 'unrelated' behavioural response when averaging across all subjects (Fig 3b, $P>0.05$). The presence
305 of rhythmic activity is a known substrate for communication between brain regions vital for
306 cognition (Fries, 2015). While rhythm power may be relevant in some cases, the key property of such
307 rhythms is to provide a temporal framework with which to coordinate activity over cortical distance.
308 We therefore next examined basic measures of this temporal framework associated with delta and
309 theta rhythms.

310 *Pairwise regional covariance metrics also revealed task- but not semantic interpretation-dependent*
311 *networks.* We measured the degree of synchrony from broadband signals as a measure of pairwise
312 regional communication between regions (Gray et al., 1989). Significant ($P<0.05$) pairwise regional
313 synchrony values for each correlation mean showed sequences of co-activation from 1st word
314 presentation to behavioural response for each subject (Fig. 3ci). A small number of local region pairs
315 in frontal and parietal areas correlated with task for $>15/17$ subjects (94%, Fig. 3ci,iii). However, no
316 long-range correlations were apparent (Fig. 3ciii) nor, again, did synchrony between any set of
317 region pairs correlate with either 'related' or 'unrelated' semantic outcome for all subjects (Fig. 3ci).

318 The above observations demonstrated that both the strongest ERP responses and the most
319 broadband-synchronous region pairs did not correspond with either the core semantic network
320 structure revealed by fMRI studies (see introduction), or the nature of the semantic decision made
321 on presentation of the word pairs. We therefore next examined the preceded pattern of theta-
322 mediated functional connectivity – the half theta period phase separation of activity between
323 regions (Mizusaki et al., 2009). Again, no common set of region pairs correlated with semantic
324 interpretation (Fig. 3di). However, compared to the 0 ms synchrony metric (Fig. 3c), a greater
325 number of region pairs were shared by >15/17 subjects (94%) when considering semantic task alone.
326 Connected regions formed a distributed network involving medial prefrontal cortex, medial frontal
327 gyrus, hippocampus, visual cortex and temporal areas. Unlike the region pairs revealed by absolute
328 synchrony, these regions have been shown previously to be vital for semantic processing - ATL-aSTG,
329 pMTG, IFG, dmPFC, IPS, AG (Whitney et al., 2011; Jefferies, 2013), Fig. 3diii), executive control -
330 vmPFC, MFG, memory - both left and right hippocampi, and task-associated primary sensory
331 processing - left and right V1 (Fig. 3diii). The resulting network was far more global than that seen for
332 zero lag/lead synchrony alone (Fig 3cii vs. Fig 3diii) and consisted of region pairs with highly
333 significant, greater anatomical separation ($P < 0.01$, $n = 6, 15$).

334 *Phase amplitude coupling (PAC) between theta and delta rhythms predicted semantic*
335 *interpretation.* The above data established that temporal interactions associated with theta rhythms
336 exposed a network of regions previously linked to semantic cognition. To investigate this further we
337 next examined any relationship between the theta rhythmic activity and the other dominant
338 component of the spectra revealed in Fig. 3a – the delta rhythm. Delta and theta rhythms show
339 cross-frequency coupling during cognition (Lakatos et al., 2005), and cross-frequency coupling in
340 general is thought to provide a temporal framework for coordinating local and distal cortical
341 dynamics (Canolty & Knight, 2010). We therefore analysed the profile of theta coupling to the delta
342 rhythm for each region. We used the mean, by region for each subject, delta rhythm phase from the
343 left hemisphere only as a reference as we wanted to prevent possible interference from inter-
344 hemispheric phase lags. The left hemisphere was chosen as previous studies have suggested a
345 dominance of the left hemisphere in semantic processing (Vigneau et al., 2006; Whitney et al.,
346 2011). Plotting the absolute (magnitude) or the theta rhythm against this mean delta phase metric
347 showed a switch from single to bi-modal peaks per delta period prior to a ‘related’ and ‘unrelated’
348 interpretation respectively. These data suggested a difference in local delta-theta phase-amplitude
349 coupling for different semantic interpretations ($P < 0.01$, Kolmogorov-Smirnov, $n = 17$, Fig. 4).

350 *A biological model predicted the changes in PAC profile correlated with altered neocortical neuronal*
351 *subtype outputs.* It is notoriously difficult to assign a genuine biological process to cross frequency
352 coupling phenomena using analytical models (Aru et al., 2015). To establish a possible neuronal
353 network mechanism to the above modification of delta-theta PAC (Fig. 4) we used an *in vitro*
354 *biological* model shown to capture delta-theta PAC previously. The model chosen generates local,
355 concurrent neocortical theta and delta rhythms in isolated parietal cortex (Carracedo et al., 2013).
356 The delta rhythm responses seen in the MEG datasets used here appeared as a consequence of
357 stimulus-locked averaging of on-going delta rhythms in individual trials ('phase resetting', Fig. 5a,b)
358 as seen previously for visual stimuli (Klein et al., 2016). It should perhaps be noted that delta
359 rhythms are a prominent feature of both slow-wave sleep *and* waking (Hall et al., 2014), with
360 amplitude differences relative to higher frequencies responsible for the subtle changes in the
361 spectral power law behaviour (Wen & Liu, 2016). We therefore first established that the model could
362 also demonstrate this phase resetting. Using thalamocortical slices, time-discrete (50 μ s) thalamic
363 stimulation (bipolar electrode, 10-100 μ A) was extremely effective at phase resetting the persistent
364 neocortical delta rhythm (Fig 5. c,d).

365 However, while phase reset is a fundamental response of on-going cortical rhythms to input, it is
366 also a potential source of spurious cross-frequency coupling measures (Aru et al., 2015). We
367 therefore designed a set of model conditions that attempted to capture potential differences in
368 cortical dynamics associated with semantic interpretation *in the absence* of discrete inputs: The *in*
369 *vitro* model is dependent on low, but non-zero, cholinergic neuromodulation. Acetylcholine levels in
370 the cortex vary on a sub-second timescale and carry information about the subjective nature of
371 sensory stimuli. This form of neuromodulation is positively correlated with stimulus presentation
372 properties, the degree of novelty, saliency and the subject's degree of attention to the stimulus
373 (Acquas et al., 1996; Baxter & Chiba, 1999). Thus we used different levels of cholinergic
374 neuromodulation to explore the effects on the profile of concurrent theta-delta rhythm interactions
375 in the three main principal neuron subtypes in deep and superficial neocortex (Fig. 6a).

376 Lower and higher levels of pharmacologically-induced cholinergic excitation (2 μ M and 6 μ M
377 carbachol respectively) generated significantly different profiles of local delta rhythm-nested
378 neuronal excitation (excitatory postsynaptic potentials - EPSPs) and response (action potential – AP -
379 generation) in all 3 neuronal subtypes tested (Fig. 6). Intrinsically bursting (IB) neurons in layer 5 (the
380 primary generators of the local neocortical delta rhythm) generated trains of action potentials
381 overlying ramped excitatory synaptic inputs (EPSPs, Fig. 6d, Fig. 8). A small but significant decrease in
382 outputs from these neurons was seen at higher cholinergic excitation ($P < 0.05$).

383 In contrast, for regular spiking (RS) neurons in layers 5 and 2/3, both EPSP inputs and AP output
384 probabilities became bimodal under higher cholinergic excitation, with dual EPSPs leading to dual,
385 discrete periods of output generation (Figs.6b,c). These dual peaks in input and output were
386 separated, on average, by one theta period within each accompanying delta period (L5 RS, 175 ± 12
387 ms, L2/3 RS, 205 ± 25 ms) – an observation similar to the peak separation in the MEG cross-frequency
388 coupling measures (Fig 4). MEG is thought to measure mean local dendritic current flow in
389 populations of neurons throughout the cortical mantle. We therefore compared the model data with
390 the subject data by pooling the mean EPSP profiles (Fig.7b) and spike probabilities (Fig. 7c) from all 3
391 neuron subtypes and compared to the global mean delta-theta PAC profile (Fig. 7a). The transition
392 from single to dual peaks was significant in each case (FDR, $P < 0.05$, Figs. 7a-ii-cii). In addition, no
393 significant difference was seen between the corresponding model and human data cross-frequency
394 coupling profiles: Those associated with ‘related’ or ‘unrelated’ semantic interpretations in subjects
395 compared with model data in low- and high-cholinergic conditions respectively ($P > 0.05$ for pooled
396 mean EPSP and AP probability measures). This suggested that reaching an ‘unrelated’ interpretation
397 for paired words involved cholinergically-mediated, dual state changes at theta frequency in RS
398 neuron inputs/outputs temporally aligned to activity in delta-generating IB neurons (see discussion).

399

400 **4. Discussion**

401 The data presented here demonstrate that theta and delta frequency dynamics dominate the
402 spectral profile of cortical activity during semantic processing. Temporal coordination at theta
403 frequency exposed the core regions of the semantic cognition network revealed by fMRI studies (see
404 introduction). Additional temporally coupled regions exposed were the task-relevant primary
405 sensory regions (bilateral V1), the hippocampi (but with the caveat that signal from deep structures
406 can be unreliable) and key control regions involved in decision-making (MFG, vmPFC). The profile of
407 delta-theta PAC within this network provided a predictor of semantic decision outcome in the word-
408 pair task used here, with PAC profile in the period from stimulus presentation to RT showing dual
409 peaks for unrelated decisions and single peaks for related decisions. Dual peaks in delta-theta PAC
410 were reproduced in a biological model in a manner dependent on cholinergic neuromodulation
411 suggesting multiple activations of cholinergically-excited theta-generating neurons were required to
412 reach an ‘unrelated’ compared to a ‘related’ semantic decision. How could such a temporal pattern
413 arise and how does it fit with current theories of the role of cross-frequency coupling in cognition?

414 Cross-frequency coordination of brain rhythms is a potent substrate for a broad range of cognitively-
415 relevant processes (Hyafil et al., 2015), and the pattern of coordination may represent a range of
416 different neuronal network architectures if it is assumed the phenomenon is biologically-generated.
417 Unfortunately, apparent interactions can be generated non-biologically in many different situations
418 related to data type, quality, analysis methods and external inputs (Aru et al., 2015). However,
419 several observations do suggest the present observations were a consequence of a biological
420 substrate:

421 a) The phase reset that generated the theta and delta average responses seen occurred on
422 presentation of the first word not the second. This may explain why ERP measures alone exposed
423 only the regions primarily receiving the sensory information (Fig. 2c) rather than those involved in
424 the semantic task – insufficient information being presented at the time of phase-reset to perform
425 any semantic computation.

426 b) The second word presentation was not time-locked to the intrinsic frequency of the delta rhythms
427 or its nested theta rhythm – 350 ms (2.9 Hz) stimulus separation cf. 2.5 Hz and 5.2 Hz respectively.

428 c) The results presented were from all the delta/theta periods occurring from stimulus presentation
429 to decision point. Pooling multiple periods of potentially cross-frequency coupled rhythms over time
430 minimises any effects of time-discrete inputs (Aru et al., 2015).

431 d) Modelling the observed pattern of cross frequency coupling reproduced the results from human
432 data with high fidelity in the *absence* of any time-discrete external inputs (Fig. 7).

433 In addition to using the model to help ablate any possible artefacts from sensory inputs contributing
434 to the results, it also allowed us to speculate on the biological origins of the cross-frequency
435 interactions seen. Despite the species, and temperature differences the model reproduced the same
436 frequency range of theta seen in MEG data and slightly slower delta frequency. Pharmacological
437 generation of theta/delta rhythms in this manner has been shown previously to work equally well in
438 human and rodent tissue *in vitro* (Carracedo et al., 2013) and the data presented here suggest that
439 the persistent rhythm in rat can be phase-reset in a similar manner to that seen in the human MEG
440 data (Fig. 5): The consequent stimulus-locked delta rhythm survived for a longer time in the model
441 than in subjects but this may be a consequence of the absence of further stimuli related to reaching
442 the decision-point that may be present in the MEG trial data.

443 The overall change in PAC profile was remarkably similar in the model and human task-dependent
444 data. In this respect the model predicted a highly discrete division of labour across the two, coupled

445 spectral components dominating the MEG signals. Theta rhythmicity, both in terms of excitatory
446 input and action potential output, was the sole property of regular spiking (RS) neocortical neurons.
447 These neurons are purely cortico-cortical in terms of their long-range projections: That is to say, they
448 communicate exclusively with their immediate neighbours *and* distal cortical regions directly. In
449 contrast, delta rhythmicity arises purely from layer 5 intrinsic bursting neurons (Carracedo et al.,
450 2013) and this principal neuron subtype projects to immediate neighbours *and* exclusively to distal
451 subcortical regions (Groh et al., 2010; Kim et al., 2015). In addition, the local mechanisms of
452 generation of these two rhythms are very different: The delta rhythm is generated in thalamus and
453 neocortex by synaptically coupled bursting neurons operating in networks controlled by GABA_B
454 receptor-mediated synaptic inhibition (Hughes et al., 1998; Carracedo et al., 2013) whereas the
455 theta rhythm (5-8 Hz) is generated by complex interactions between fast and slow GABA_A receptor-
456 mediated inhibitory synaptic inputs to principal cells (Gillies et al., 2002).

457 This division of labour has at least two consequences for the dynamical differences shown here prior
458 to reaching a semantic decision: Firstly, the observed bimodal nature of deep and superficial layer RS
459 neuronal output probabilities, separated by one theta period, would suggest a role in reinforcing
460 interaction between local cortical layers. Reciprocal interactions between deep and superficial layers
461 has been proposed to represent a biological substrate for unsupervised learning and recall in layered
462 neural networks (Dayan et al., 1995; Carracedo et al., 2013). Longer range cortico-cortical
463 interactions at theta frequency are also suggested to underlie error detection with reference to
464 memory (Jensen & Tesche, 2002; Jacobs et al., 2006), and in prefrontal, medial frontal and parietal
465 areas (Luu et al., 2004; Trujillo & Allen, 2007; van Driel et al., 2012). These regions formed part of the
466 task-related circuit revealed by theta-related region coupling (Fig. 3d). This suggested a commonality
467 between error signalling and the 'actual vs. expected' nature of the comparison between 1st and 2nd
468 presented words in the task. The overt 'state-change'-like nature of the output probabilities in RS
469 neurons resembled activity patterns shown in orbitofrontal neurons during subjective decision-
470 making previously (Rich & Wallis, 2016) (Fig. 8).

471 Secondly, the theta-frequency state changes seen in RS neurons were strongly phase-related to the
472 delta rhythm manifest in IB neurons. Outputs from this cell subtype target subcortical structures
473 such as colliculus, striatum and thalamus, all of which have been shown to be involved in decision-
474 making. The ramped inputs to IB neurons during delta in the model presented here closely
475 resembled those inferred from existing models of neuronal dynamics during decision-making (see
476 introduction, Hunt et al., 2012, Fig. 8). However, in these models the ascending ramp of magnitude
477 of excitation to 'decision' arises predominantly from the sensory input containing the 'values' used

478 for choice. How can this be replicated in a model that has no sensory input (the isolated parietal
479 cortex preparation)? The nature of the model indicated that ‘ramps’ in excitatory synaptic input
480 were generated locally within neocortex via feedforward interactions between slow (predominantly
481 NMDA receptor-mediated) recurrent connections between adjacent IB neurons. This fits the known
482 profile of excitatory connections to neocortical neurons: Only approximately 5% of inputs to
483 neocortical cells arise from ascending cortical input, even in primary sensory areas (Peters & Payne,
484 1993), and it is considered extremely rare to find a neuron that actually responds to a single sensory
485 stimulus or stimulus property (Abeles, 1988). The vast majority of inputs arise from local and distal
486 cortical efferents (Young, 2000). Thus the ‘ramp’ of inputs is best considered an intrinsic property of
487 cortical networks, with the cortical regional profile of sensory input dictating the onset and gradient
488 of the ‘ramp’ - the degree and spatial extent of phase reset of the on-going delta rhythm (e.g. Fig.
489 3a).

490 The strong correlation between semantic decision outcome and the profile of theta-delta cross-
491 frequency coupling suggested that the above two phenomena need to interact to perform this
492 cognitive task. The model used here suggested that cholinergic neuromodulation was critical in
493 shaping this interaction. While cholinergic responses are the rule rather than the exception in all
494 neocortical neuron subtypes the converse – neocortical neurons influencing cholinergic neuronal
495 excitability – is very rare. Interestingly, the one neocortical region shown to have a relatively strong
496 influence on the magnitude of cholinergic neuronal activity is the orbitofrontal cortex (Do et al.,
497 2016). This suggests a feedforward relationship between ‘state-change’ activity (i.e. periodic, theta
498 frequency alterations in output probability (Rich & Wallis, 2016)) in this area and the extent of
499 cholinergic drive mediating theta-frequency state changes in wider neocortex. Thus modulation of
500 the model local circuit via cholinergic excitation may not be solely related to attention and stimulus
501 novelty (Acquas et al., 1996), but also to the on-going activity associated with semantic processing
502 within neocortex.

503 We suggest that state change (Rich & Wallis, 2016) and accumulator models (Wang, 2002) may
504 therefore reflect two temporally coherent, exquisitely self-governing dynamic signatures of the
505 same local neocortical circuits synergistically modifying both local and brain-wide neuronal activity
506 prior to semantic decision. In the present data these dynamic signatures were manifest as theta and
507 delta frequency rhythms arising from different neuronal subtypes. The projection profile of these
508 neurons suggested that cross-frequency coupling may not be just facilitating simultaneous
509 interactions over different spatial scales, but rather coordinating cortico-cortical and cortico-
510 subcortical interactions. These rhythms represented the majority of the spectral content of the MEG

511 data between stimulus presentation and decision timepoint. However, they also occur coupled to
512 faster frequencies (e.g. Lakatos et al., 2005) that have also been linked to semantic processing in key
513 brain areas (Mollo et al., 2017). More comprehensive studies, over a broader dynamic range will
514 therefore likely reveal much richer detail of the semantic decision process and the role of cross-
515 frequency coupling in brain-wide communication in general.

516

517 **Disclosures.** The authors declare no competing financial interests.

518

519 **Acknowledgements.** Supported by the Wellcome Trust, IBM, NIH/NINDS R01NS044133, and the ERC
520 (SEMBIND, FLEXSEM).

521

522

523 **References**

- 524 Abeles, M. (1988) Neural codes for higher brain function. In: Markowitsch, H.J., ed. Information
525 processing by the brain. Stuttgart; Hans Huber. pp225-238.
- 526 Acquas E, Wilson C, Fibiger HC. (1996) Conditioned and unconditioned stimuli increase frontal
527 cortical and hippocampal acetylcholine release: effects of novelty, habituation, and fear. *J Neurosci*
528 16: 3089-96. PMID: 8622138.
- 529 van Ackeren MJ, Rueschemeyer SA (2014) Cross-modal integration of lexicon-semantic features
530 during word processing: evidence from oscillatory dynamics during EEG. *PLOS One* 9(7): e101042.
531 DOI: 10.1371/journal.pone.0101042.
- 532 Akam T, Kullmann DM (2010) Oscillations and filtering networks support flexible routing of
533 information. *Neuron* 67:308-20. doi: 10.1016/j.neuron.2010.06.019
- 534 Arnal LH, Giraud AL. (2012) Cortical oscillations and sensory predictions. *Trends Cogn Sci.* 16:390-8.
535 doi: 10.1016/j.tics.2012.05.003
- 536 Aru J, Aru J, Priesemann V, Wibral M, Lana L, Pipa G, Singer W, Vicente R. (2015) Untangling cross-
537 frequency coupling in neuroscience. *Curr Opin Neurobiol.*31:51-61. DOI:
538 10.1016/j.conb.2014.08.002.
- 539 Badre B, Poldrack BA, Paré-Blagoev EJ, Insler RZ, Wagner AD (2005) Dissociable Controlled Retrieval
540 and Generalized Selection Mechanisms in Ventrolateral Prefrontal Cortex. *Neuron* 47: 907-918. DOI:
541 10.1016/j.neuron.2005.07.023.
- 542 Bankó EM, Gál V, Körtvélyes J, Kovács G, Vidnyánszky Z (2011) Dissociating the effect of noise on
543 sensory processing and overall decision difficulty. *J Neurosci.* 31:2663-74. doi:
544 10.1523/JNEUROSCI.2725-10.2011.
- 545 Başar E, Başar-Eroglu C, Karakaş S, Schürmann M (2001) Gamma, alpha, delta, and theta oscillations
546 govern cognitive processes. *Int J Psychophysiol.* 39:241-8. PMID: 11163901.
- 547 Binder JR, Desai RH, Graves WW, Conant LL (2009) Where is the semantic system? A critical review
548 and meta-analysis of 120 functional neuroimaging studies. *Cerebral Cortex* 19: 2767-2796. DOI:
549 10.1095/cercor/bhp055.
- 550 Calderone DJ, Lakatos P, Butler PD, Castellanos FX. (2014) Entrainment of neural oscillations as a
551 modifiable substrate of attention. *Trends Cogn Sci.* 18:300-9. DOI: 10/1016/j.tics.2014.02.005
- 552 Canolty RT, Knight RT (2010) The functional role of cross-frequency coupling. *Trends Cogn Sci* 14:
553 506-15. DOI: 10.1016/j.tics.2010.09.001.

554 Carracedo LM, Kjeldsen H, Cunnington L, Jenkins A, Schofield I, Cunningham MO, Davies CH, Traub,
555 RD, Whittington MA (2013) A neocortical delta rhythm facilitates reciprocal interlaminar interactions
556 via nested theta rhythms. *J Neurosci* 33: 10750-61. DOI: [10.1523/JNEUROSCI.0735-13.2013](https://doi.org/10.1523/JNEUROSCI.0735-13.2013).

557 Christoff K, Gordon AM, Smallwood J, Smith R, Schooler JW (2009) Experience sampling during fMRI
558 reveals default network and executive system contributions to mind wandering. *Proc Natl Acad Sci U*
559 *S A* 106:8719-24. doi: [10.1073/pnas.0900234106](https://doi.org/10.1073/pnas.0900234106).

560 Cobb SR, Buhl EH, Halasy K, Paulsen O, Somogyi P. (1995). Synchronization of neuronal activity in
561 hippocampus by individual GABAergic interneurons. *Nature* 378:75-8. DOI: [10.1038/378075a0](https://doi.org/10.1038/378075a0).

562 Corbett F, Jefferies E, Eshan S, Lambon Ralph MA. (2009) Different impairments of semantic
563 cognition in semantic dementia and semantic aphasia: Evidence from the non-verbal domain. *Brain*
564 132: 2593-2608. DOI: [10.1093/brain/awp146](https://doi.org/10.1093/brain/awp146).

565 Dayan P, Hinton GE, Neal RM, Zemel RS (1995) The Helmholtz machine. *Neural Comput* 7: 889-904.
566 PMID: 7584891

567 van Driel J, Ridderinkhof KR, Cohen MX (2012) Not all errors are alike: theta and alpha EEG dynamics
568 relate to differences in error-processing dynamics. *J Neurosci* 32: 16795-806. DOI:
569 [10.1523/JNEUROSCI.0802-12.2012](https://doi.org/10.1523/JNEUROSCI.0802-12.2012)

570 Do JP, Xu M, Lee SH, Chang WC, Zhang S, Chung S, Yung TJ, Fan JL, Miyamichi M, Luo L, Dan Y (2016)
571 Cell type-specific long-range connections of basal forebrain circuit. *Elife* 5. pii: e13214. doi:
572 [10.7554/eLife.13214](https://doi.org/10.7554/eLife.13214).

573 Duncan J (2010) The multiple-demand (MD) system of the primate brain: Mental programs for
574 intelligent behavior. *Trends Cog Sci* 14: 172-179. DOI: [10.1016/j.tics.2010.01.004](https://doi.org/10.1016/j.tics.2010.01.004).

575 Fries P (2015) Rhythms for cognition: Communication through coherence. *Neuron* 88: 220–235. DOI:
576 [10.1016/j.neuron.2015.09.034](https://doi.org/10.1016/j.neuron.2015.09.034).

577 Gillies MG, Traub RD, LeBeau FE, Davies CH, Gloveli T, Buhl EH, Whittington MA (2002) A model of
578 atropine-resistant theta oscillations in rat hippocampal area CA1. *J Physiol.* 15: 779-93. PMID
579 12231638.

580 Gray CM, König P, Engel AK, Singer W (1989) Oscillatory responses in cat visual cortex exhibit inter-
581 columnar synchronization which reflects global stimulus properties. *Nature* 338: 334-337. PMID
582 2922061

583 Groh A, Meyer HS, Schmidt EF, Heintz N, Sakmann B, Krieger P (2010) Cell-type specific properties of
584 pyramidal neurons in neocortex underlying a layout that is modifiable depending on the cortical
585 area. *Cereb Cortex* 20: 826-36. DOI: [10.1093/cercor/bhp152](https://doi.org/10.1093/cercor/bhp152)

586 Hall TM, de Carvalho F, Jackson A (2016) A Common Structure Underlies Low-Frequency Cortical
587 Dynamics in Movement, Sleep, and Sedation. *Neuron* 83: 1185–1199. doi:
588 [10.1016/j.neuron.2014.07.022](https://doi.org/10.1016/j.neuron.2014.07.022)

589 Harmony T (2013) The functional significance of delta oscillations in cognitive processing. *Front*
590 *Integr Neurosci.* 7:83. doi: [10.3389/fnint.2013.00083](https://doi.org/10.3389/fnint.2013.00083).

591 Huang MX, Mosher JC, Leahy RM (1999) A sensor-weighted overlapping-sphere head model and
592 exhaustive head model comparison for MEG. *Phys Med Biol* 44: 423-40. PMID 10070729

593 Hughes SW, Crunelli V (1998) Dynamic clamp study of Ih modulation of burst firing and delta
594 oscillations in thalamocortical neurons in vitro. *Neuroscience* 87: 541-550. PMID 9758221.

595 Hunt LT, Kolling N, Soltani A, Woolrich MW, Rushworth MF, Behrens TE (2012) Mechanisms
596 underlying cortical activity during value-guided choice. *Nat Neurosci* 15: 470-6. DOI:
597 [10.1038/nn.3017](https://doi.org/10.1038/nn.3017).

598 Hyafil A, Giraud AL, Fontolan L, Gutkin B. (2015) Neural Cross-Frequency Coupling: Connecting
599 Architectures, Mechanisms, and Functions. *Trends Neurosci.* 38:725-740. DOI:
600 [10.1016/j.tins.2015.09.001](https://doi.org/10.1016/j.tins.2015.09.001).

601 Jacobs J, Hwang G, Curran T, Kahana MJ (2006) EEG oscillations and recognition memory: theta
602 correlates of memory retrieval and decision making. *Neuroimage* 32: 978-87. DOI:
603 [10.1016/j.neuroimage.2006.02.018](https://doi.org/10.1016/j.neuroimage.2006.02.018).

604 Jefferies, E (2013) The neural basis of semantic cognition: Converging evidence from
605 neuropsychology, neuroimaging and TMS. *Cortex* 49: 611–625. DOI: [10.1016/j.cortex.2012.10.008](https://doi.org/10.1016/j.cortex.2012.10.008).

606 Jensen O, Tesche CD (2002) Frontal theta activity in humans increases with memory load in a
607 working memory task. *Eur J Neurosci* 15: 1395-9. DOI: [10.1046/j.1460-9568.2002.01975.x](https://doi.org/10.1046/j.1460-9568.2002.01975.x)

608 Kim EJ, Juavinett AL, Kyubwa EM, Jacobs MW, Callaway EM (2015) Three Types of Cortical Layer 5
609 Neurons That Differ in Brain-wide Connectivity and Function. *Neuron* 88: 1253-67. DOI:
610 [10.1016/j.neuron.2015.11.002](https://doi.org/10.1016/j.neuron.2015.11.002)

611 Klein C, Evrard HC, Shapcott KA, Haverkamp S, Logothetis NK, Schmid MC (2016). Cell Targeted
612 Optogenetics and Electrical Microstimulation Reveal the Primate Koniocellular Projection to Supra-
613 granular Visual Cortex *Neuron* 90: 143–151. DOI: [10.1016/j.neuron.2016.02.036](https://doi.org/10.1016/j.neuron.2016.02.036).

614 Klimesch W, Schimke H, Schwaiger J (1994) Episodic and semantic memory: an analysis in the EEG
615 theta and alpha band. *Electroencephalogr Clin Neurophysiol* 91:428-41. PMID 7529682.

616 Klimesch W (2012) α -band oscillations, attention, and controlled access to stored information.
617 *Trends Cogn Sci.* 16:606-17. doi: 10.1016/j.tics.2012.10.007.

618 Koelsch S, Kasper E, Sammler D, Schulze K, Gunter T, Friederici AD (2004) Music, language and
619 meaning: brain signatures of semantic processing. *Nat Neurosci* 7: 302-307. DOI: 10.1038/nn1197.

620 Kopell N, Ermentrout GB, Whittington MA, Traub RD (2000) Gamma rhythms and beta rhythms have
621 different synchronizing properties. *Proc Natl Acad Sci USA* 97: 1867-72. PMID 10677548.

622 Kozinska D, Carducci F, Nowinski K (2001) Automatic alignment of EEG/MEG and MRI data sets. *Clin*
623 *Neurophysiol* 112: 1553–1561. PMID: 11459696

624 Kramer MA, Eden UT (2013) Assessment of cross-frequency coupling with confidence using
625 generalized linear models. *J Neurosci Meth* 220: 64-74. DOI: [10.1016/j.jneumeth.2013.08.006](https://doi.org/10.1016/j.jneumeth.2013.08.006)

626 Lakatos P, Shah AS, Knuth KH, Ulbert I, Karmos G, Schroeder CE (2005) An Oscillatory Hierarchy
627 Controlling Neuronal Excitability and Stimulus Processing in the Auditory Cortex. *J Neurophysiol* 94:
628 1904-1911. DOI: [10.1152/jn.00263.2005](https://doi.org/10.1152/jn.00263.2005).

629 Li A, Cornelius SP, Liu YY, Wang L, Barabasi AL (2017) The fundamental advantages of temporal
630 networks. *Science* 258: 1042-1046. DOI: 10.1126/science.aai7488.

631 Luu P, Tucker DM, Makeig S (2004) Frontal midline theta and the error-related negativity:
632 neurophysiological mechanisms of action regulation. *Clin Neurophysiol* 115: 1821-35. DOI:
633 [10.1016/j.clinph.2004.03.031](https://doi.org/10.1016/j.clinph.2004.03.031)

634 Mizuseki K, Sirota A, Pastalkova E, Buzsáki G (2009) Theta oscillations provide temporal windows for
635 local circuit computation in the entorhinal-hippocampal loop. *Neuron* 64:267-80. doi:
636 10.1016/j.neuron.2009.08.037

637 Mollo G, Cornelissen PL, Millman RE, Ellis AW, Jefferies E (2017). Oscillatory dynamics supporting
638 semantic cognition: MEG evidence for the contribution of anterior temporal lobe hub and modality-
639 specific spokes. *PLOS One* 12(1): e0169269.

640 Nácher V, Ledberg A, Deco G, Romo R (2013) Coherent delta-band oscillations between cortical
641 areas correlate with decision making. *Proc Natl Acad Sci USA* 110: 15085-90. DOI:
642 [10.1073/pnas.1314681110](https://doi.org/10.1073/pnas.1314681110).

643 Patterson K, Nestor PJ, Rogers TT (2007) Where do you know what you know? The representation of
644 semantic knowledge in the human brain. *Nat Rev Neurosci* 8:976-987.

645 Peters A, Payne BR (1993) Numerical relationships between geniculocortical afferents and pyramidal
646 cell modules in cat primary visual cortex, *Cerebral Cortex* 1: 69–78.

647 van Petten C, Luka BJ (2006) Neural localisation of semantic context effects in electromagnetic and
648 hemodynamic studies. *Brain lang* 97: 297-293.

649 Purcell BA, Heitz RP, Cohen JY, Schall JD, Logan GD, Palmeri TJ (2010) Neurally constrained modeling
650 of perceptual decision making. *Psychol Rev* 117: 1113-43. DOI: [10.1037/a0020311](https://doi.org/10.1037/a0020311).

651 Ralph MA, Jefferies E, Patterson K, Rogers TT (2017) The neural and computational bases of semantic
652 cognition. *Nat Rev Neurosci.* 18:42-55. doi: 10.1038/nrn.2016.150.

653 Remondes M, Wilson MA (2013) Cingulate-hippocampus coherence and trajectory coding in a
654 sequential choice task. *Neuron* 80:1277-89. doi: 10.1016/j.neuron.2013.08.037.

655 Rich EL, Wallis JD (2016) Decoding subjective decisions from orbitofrontal cortex. *Nat Neurosci* 19:
656 973-980. DOI: [10.1038/nn.4320](https://doi.org/10.1038/nn.4320).

657 Roopun AK, Kramer MA, Carracedo LM, Kaiser M, Davies CH, Traub RD, Kopell NJ, Whittington MA
658 (2008) Temporal Interactions between Cortical Rhythms. *Front Neurosci.* 2:145-54. doi:
659 10.3389/neuro.01.034.2008.

660 Schwartz MF, Kimberg DY, Walker GM, Brecher A, Faseyitan OK, Dell GS (2011) Neuroanatomical
661 dissociation for taxonomic and thematic knowledge in the human brain. *Proc Natl Acad Sci USA*
662 108: 8520-8424.

663 Sharot T, Kanai R, Marston D, Korn CW, Rees G, Dolan RJ (2012) Selectively altering belief formation
664 in the human brain. *Proc Natl Acad Sci USA* 109: 17058-62.

665 Storey JD, Tibshirani R (2003) Statistical significance for genomewide studies. *Proc Natl Acad Sci USA*
666 100: 9440-9445

667 Trujillo LT, Allen JJ (2007) Theta EEG dynamics of the error-related negativity. *Clin Neurophysiol* 118:
668 645-68. DOI: [10.1016/j.clinph.2006.11.009](https://doi.org/10.1016/j.clinph.2006.11.009)

669 Van Veen BD (1997) Localization of brain electrical activity via linearly constrained minimum
670 variance spatial filtering. *IEEE Transactions on Biomed Eng* 44: 867-880. DOI: [10.1109/10.623056](https://doi.org/10.1109/10.623056)

671 Vigneaua, M., Beaucousina, V., Hervéa, P.Y., Duffauc, H., Crivelloa, F., Houdéa, O., Mazoyera, B.,
672 Tzourio-Mazoyera, N., 2006. Meta-analyzing left hemisphere language areas: Phonology, semantics,
673 and sentence processing. *Neuroimage* 30, 1414-1432. DOI: [10.1016/j.neuroimage.2005.11.002](https://doi.org/10.1016/j.neuroimage.2005.11.002)

674 Visser M, Jefferies E, Lambon Ralph MA (2010) Semantic processing in the anterior temporal lobes: a
675 meta-analysis of the functional neuroimaging literature. *J Cogn Neurosci*. 22:1083-94. doi:
676 10.1162/jocn.2009.21309

677 Wang XJ (2002) Probabilistic decision making by slow reverberation in cortical circuits. *Neuron* 36:
678 955-968.

679 Wen H, Liu Z (2016) Separating Fractal and Oscillatory Components in the Power Spectrum of
680 Neurophysiological Signal. *Brain Topography* 29: 13-26. doi: 10.1007/s10548-015-0448-0

681 Whitney C, Kirk M, O'Sullivan J, Lambon Ralph MA, Jefferies E (2011) The Neural Organization of
682 Semantic Control: TMS Evidence for a Distributed Network in Left Inferior Frontal and Posterior
683 Middle Temporal Gyrus. *Cerebral Cortex* 21: 1066-1075. DOI: 10.1093/cercor/bhq180.

684 Wilson M (1988) MRC psycholinguistic database: Machine-usable dictionary, version 2.00. *Behavior*
685 *Research Methods, Instruments, & Computers* 20: 6-10. DOI: 10.3758/BF03202594.

686 Young MP (2000) The architecture of visual cortex and inferential processes in vision. *Spatial Vision*
687 13: 137–146.

688

689 **Figure legends.**

690 **Figure 1. Example of methods used to quantify activity alone and by phase of delta and theta**
691 **oscillation. a)** Example trace showing a single region's mean (over trials) response pattern.
692 Activation of the region was quantified as deviations of the MEG signal greater than +2SD above the
693 mean. Scale bar 2 nA.m, 200 ms. **bi)** Example cross-covariogram (meaned over trials) for a single pair
694 of regions in one subject over the timecourse shown for a). Time-variant cross-covariance was taken
695 either at 0 ms delay or one half a theta period delay. **bii)** Example of a time-variant cross-correlation
696 at 0 ms from bi illustrating the thresholding used to define coactivation. Scale bar 0.2 normalised
697 covariance units, 200 ms. **c)** Left panel: Example delta (black line) and theta (grey line) band-passed
698 activity (1-4 Hz and 4.5-7.5 Hz respectively). Data shows the averages for all left cortical regions for
699 one subject. Scale bar 0.5 nA.m, 200 ms. Right panel: Simulation of the effect of theta magnitude
700 modulation (blue) by a single 'delta' gaussian. The resulting phase-amplitude coupling metric is
701 shown in red.

702 **Figure 2: Raw response magnitude demonstrates common regions related to subjective task**
703 **performance but does not predict outcome. a)** Pictorial examples from the task. **b)** Percentage
704 errors and reaction times post second stimulus for all subjects for the two conditions – related
705 (black) and unrelated (red). **ci)** An example of region activity changes with time. Data from one
706 subject, averaged for 'related' trials is displayed as colormap where regions form each row (arranged
707 by time to maximal response). Trial time is along the x-axis and MEG region activations (>2SD) are on
708 the colour axis. Times for stimulus onset are shown as dashed lines. Note region numbers (y-axis)
709 were reorganised by time of initial activation and do not represent the numbers given in methods.
710 **cii)** Plot shows the number of active regions (>2SD from the mean signal from 0.8-2.0s) across
711 subject. Note no regions were common to more than 7/17 subjects when considering outcome
712 ('related' – black line, 'unrelated' – red line, 'related' and 'unrelated' – blue line). **ciii)** Map shows the
713 location of each of the 10 regions found common to >15 subjects (94%) overlaid on a horizontal
714 brain representation viewed from below.

715 **Figure 3. Synchrony and theta covariance differentially demonstrate common region pairs related**
716 **to subjective task performance but do not predict outcome. a)** Average waveform (left) and
717 spectrograms (right) for 4 example regions (LPCC, LAG, RAIC and RpMTG) averaged over all trials for
718 one example subjects for the related (black) and unrelated (red) conditions. Scale bar = 200 ms,
719 2nA.m. **b)** Mean (by subject) difference between 'related' and 'unrelated' delta and theta power
720 shown as colormap of percent difference calculated for each point of grid of beamformed nodes
721 with 5mm spacing throughout the brain. Note none of these regional differences was significant

722 when corrected for multiple comparisons (FWE $p < 0.05$ in SPM). **ci**) Pairwise, normalised cross-
723 covariance between regions demonstrated trajectories of synchrony above threshold ($>2SD$) from
724 stimulus presentation (inset). Note region numbers (y-axis) were reorganised by time of initial
725 activation and do not represent the numbers given in methods. Main graph shows number of region
726 pairs with correlations $> 2 SD$ above mean for each behavioural outcome. No synchronous region
727 pairs were common to >8 subjects when separated into outcome ('related' – black line, 'unrelated' –
728 red line). 0 ms synchrony showed only 5 region pairs interacted in >15 subjects when considering
729 task (blue line). **cii**) cross-covariance matrix of all region pairs, colormapped onto commonality
730 across the subject pool. **ciii**) Location of each of the 5 region pairs common to >15 (94%) of subjects.
731 **di**) Theta covariance between regions demonstrated trajectories from stimulus presentation (inset).
732 Main graph shows number of region pairs with theta-lagged correlations $> 2 SD$ above mean for each
733 behavioural outcome. Theta covariance showed 14 region pairs interacted in >15 subjects when
734 considering task (blue line). **dii**) cross-covariance matrix of all region pairs, colormapped onto
735 commonality across subjects. Dark colours cf. light colours indicate commonality in greater numbers
736 of subjects. **diii**) Location of each of the 14 region pairs common to >15 (94%) or subjects. Inset
737 shows the distribution of inter-regional distances for interacting regions in each case. Note the
738 significant ($P < 0.05$) shift from short to long-distance functional connections when considering theta
739 covariance (orange) vs. synchrony (purple).

740 **Figure 4. The profile of delta/theta phase amplitude coupling predicted semantic interpretation.**
741 Phase-amplitude coupling of region-averaged data, filtered for theta magnitude (4.5 – 7.5 Hz), with
742 reference to the mean delta rhythm phase. The cross-frequency coupling profiles were significantly
743 different ($P < 0.05$, $n=17$, Kolmogorov-Smirnov) when comparing activity prior to a 'related' (black)
744 vs. an 'unrelated' (red) interpretation. Inset shows significant PAC epochs polar plotted by delta
745 phase.

746 **Figure 5. Stimulus-induced delta rhythms are generated by phase reset. a.** Example, non-averaged
747 single traces from a single subject ($n=92$ trials). Upper figure shows the beamformed signal from
748 LAG. Individual trial responses are shown in black, average in red. Stimuli were presented at the
749 times indicated by the arrows. Middle figure shows a single example of raw data (black) and the
750 corresponding filtered data (blue) to illustrate the continual presence of delta activity pre- and post
751 trial. Lower figure shows the phase for each of the 92 signals (black) and the average phase (red). **b.**
752 Spectrograms constructed from 'a' in two different ways: Upper spectrogram shows the power in
753 the broadband signal derived from the average of each single trial. Lower spectrogram shows the
754 power from the averaged signal. Note the stimulus-induced delta power increase is only apparent

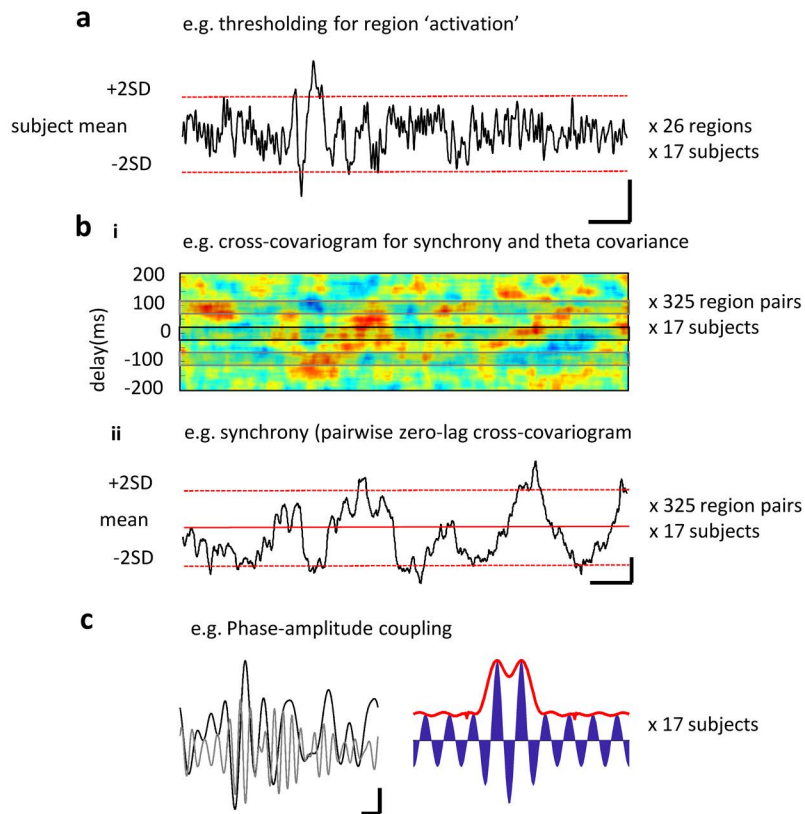
755 from the average signal, the actual delta activity is persistent. **c.** *In vitro* model of persistent delta
756 rhythms reproduced the stimulus-induced phase reset of persistent delta rhythms. Upper figure
757 shows the signal from parietal cortex aligned to electrical; stimulation of thalamus in thalamocortical
758 slices. Individual signals shown in black, the stimulus-aligned average is shown in red. Lower figure
759 shows the corresponding phase of the recorded oscillation. **d.** Phase reset plot for thalamic input to
760 parietal cortex in the model. Note the highly linear, 'near absolute' nature of the phase reset.

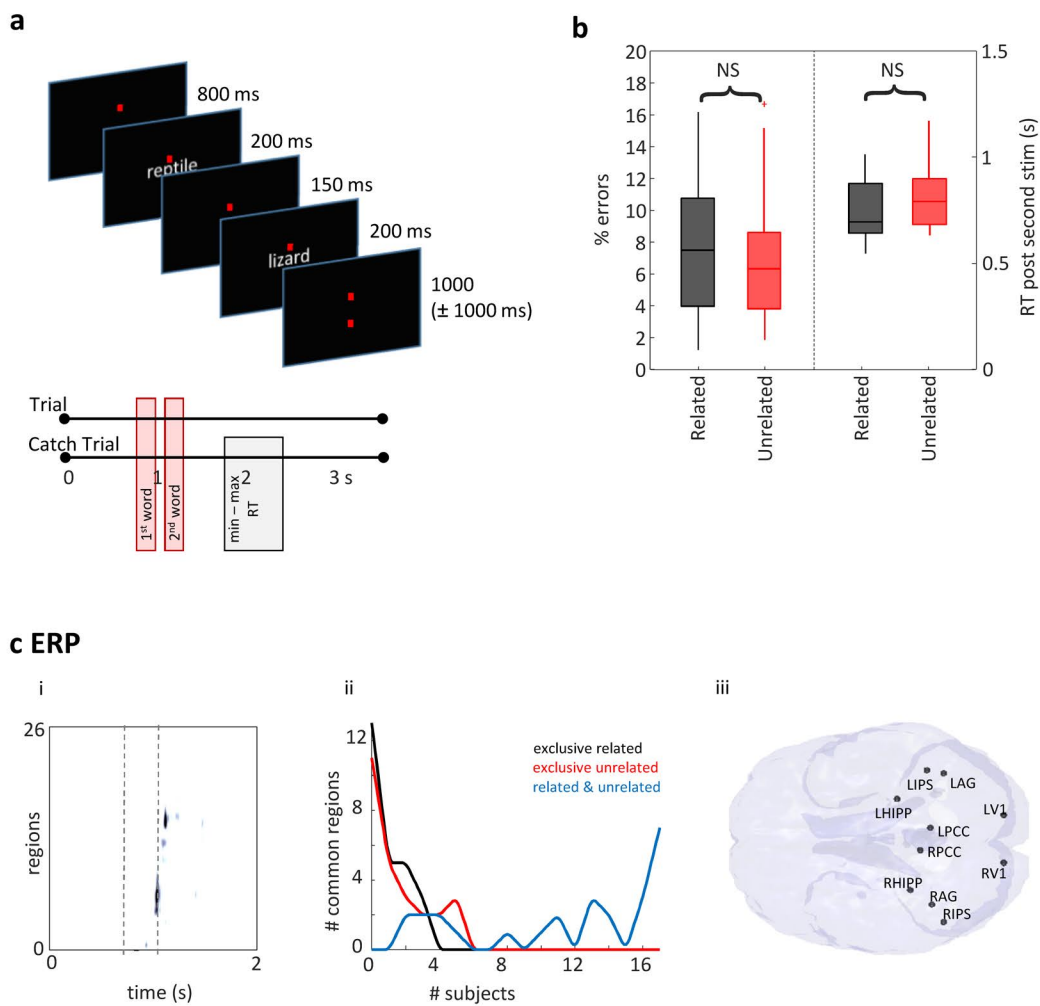
761 **Figure 6: Biological model of concurrent theta/delta activity reproduces MEG outcome-specific**
762 **dynamics via altered cholinergic excitation.** **a)** schematic of cells targeted in the *in vitro* parietal
763 cortex slice. Regular spiking (RS) neurons were recorded in layer 2/3 and layer 5, Intrinsically
764 bursting (IB) neurons were recorded in layer 5. Spontaneous delta activity was recorded in the
765 presence of cholinergic agonist (carbachol) at two different concentrations (2 μ M, black lines, 6 μ M,
766 red lines). **b)** Mean \pm s.e.mean probability of action potential generation in layer 2/3 RS neurons
767 binned according to phase of layer 5 field potential delta rhythm. Significantly larger action potential
768 probabilities ($p < 0.05$, $n = 10$ replicates per $N = 5$ slices/neurons) were seen for the higher level of
769 cholinergic excitation from 30-90° (asterisk). Example traces show activity at resting membrane
770 potential (spikes, upper examples) and at -70 mV (EPSPs, lower examples). **c)** A similar profile of
771 action potential output changes was seen when comparing outputs from layer 5 RS neurons. **d)**
772 Action potential bursts dominated layer 5 IB neuron activity. Elevated cholinergic excitation
773 significantly reduced these burst outputs (asterisk, $p < 0.05$, $n = 10$ replicates per $N = 5$ slices/neurons).

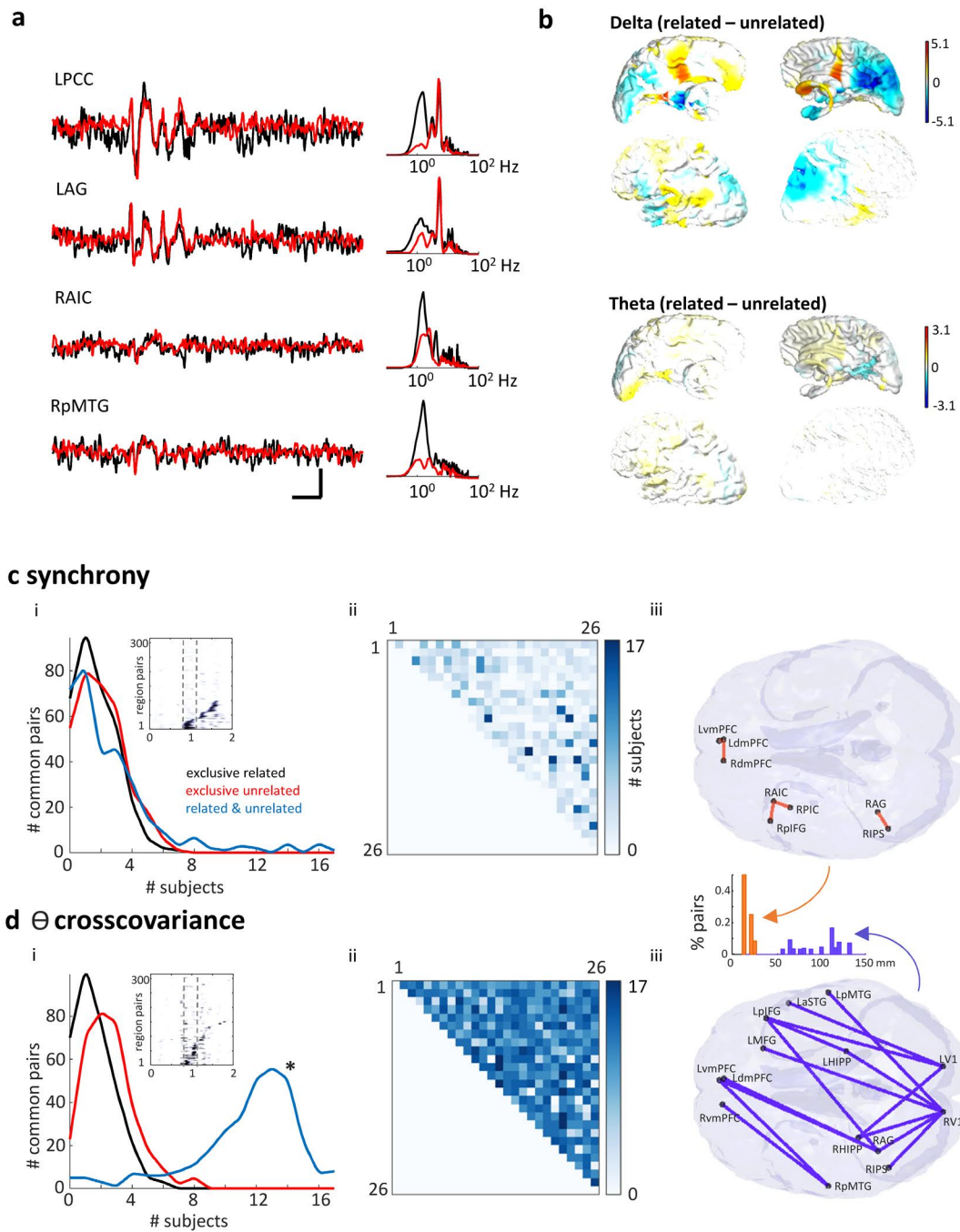
774 **Figure 7. Neuronal EPSP (input) and action potential generation (output) profiles match**
775 **theta/delta cross-frequency coupling profile differences for 'related' vs. 'unrelated' semantic**
776 **interpretations.** Decision dependent differences in MEG theta-delta cross-frequency coupling (**a**)
777 were not significantly different from the mean EPSP profiles (**b**) and Action potential (**c**) profiles
778 pooled from all 3 neuron subtypes ($P > 0.05$, Kolmogorov-Smirnov, MEG 'related' vs. model lower
779 cholinergic excitation (black), and MEG 'unrelated' vs. model higher cholinergic excitation (red).
780 Lower graphs show polar plots for values in the upper-quartile range of the distribution. Note the
781 presence of an additional peak later in the delta period when comparing the two outcomes/model
782 conditions.

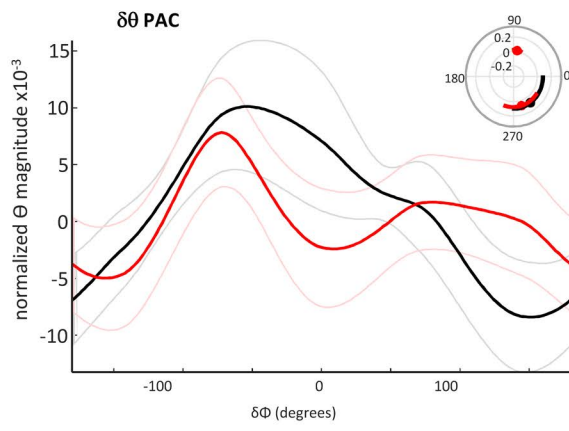
783 **Figure 8. Biological model predicts theta rhythm involvement in cortico-cortical communication**
784 **and delta rhythm involvement in cortical-subcortical communication.** **Upper panel:** Layer 5 IB
785 neuronal behaviour in the experimental model of coupled theta and delta activity displayed overt
786 ramp-like EPSPs indicative of increasing synaptic drive during the active part of one delta rhythm
787 duty cycle. This behaviour resembled that of accumulator neurons used to model decision-making.

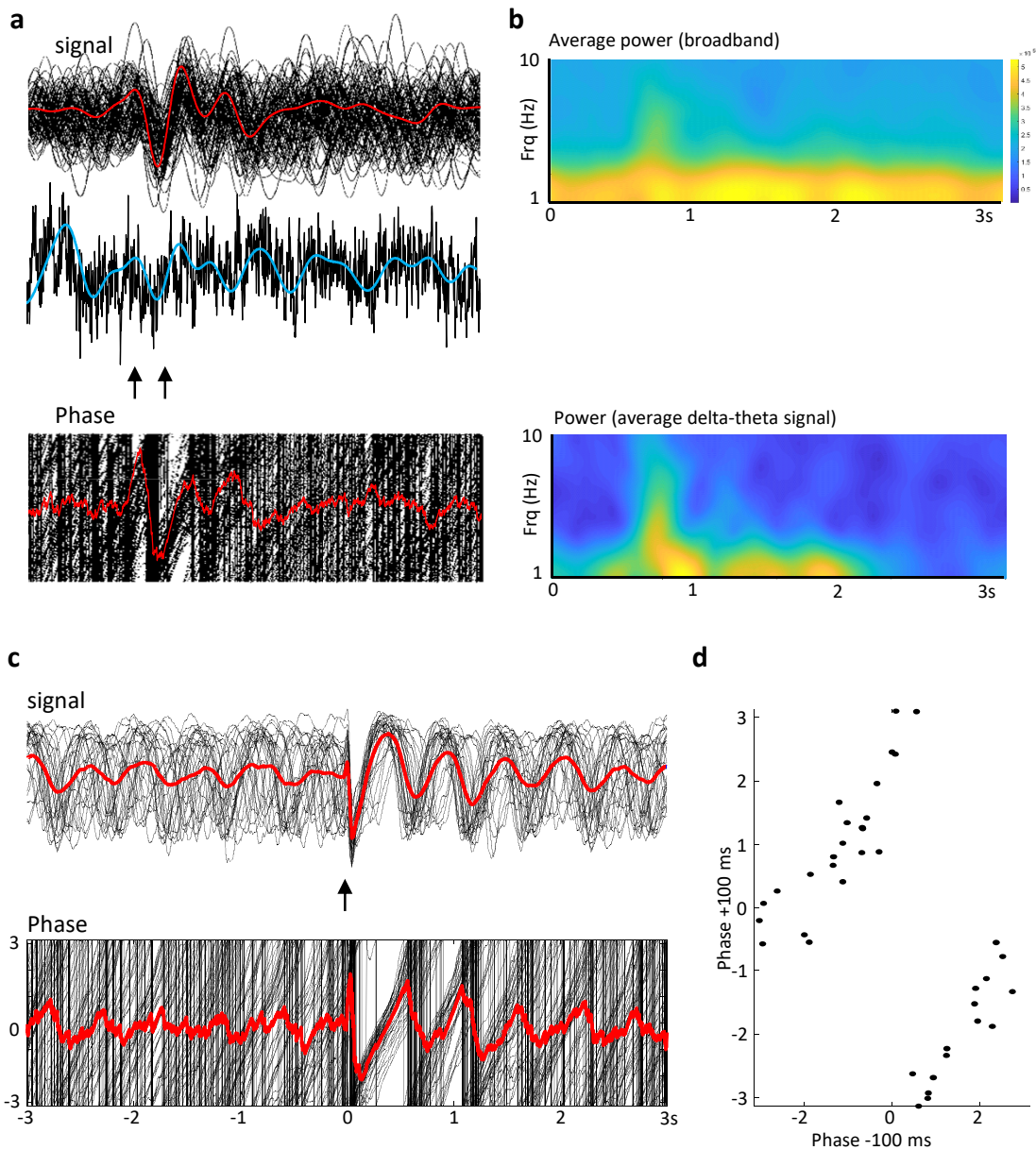
788 These neurons are all subcortically-projecting in neocortex (Groh et al.,2010; Kim et al., 2015).
789 Accumulator model figure was adapted from Hunt et al.,2012. **Lower panel:** Layer 5 and layer 2/3 RS
790 neuronal behaviour in the experimental model showed state-like changes in action potential output
791 probabilities driven by multiple EPSP inputs in a manner dependent on subsequent decision. Similar
792 changes in the probability of neuronal activity were reported for frontal cortical neurons using linear
793 discriminant analysis (LDA) of unit activity. LDA probability figure adapted from Rich & Wallis, 2016.
794 RS neurons are exclusively cortico-cortical projecting neurons.

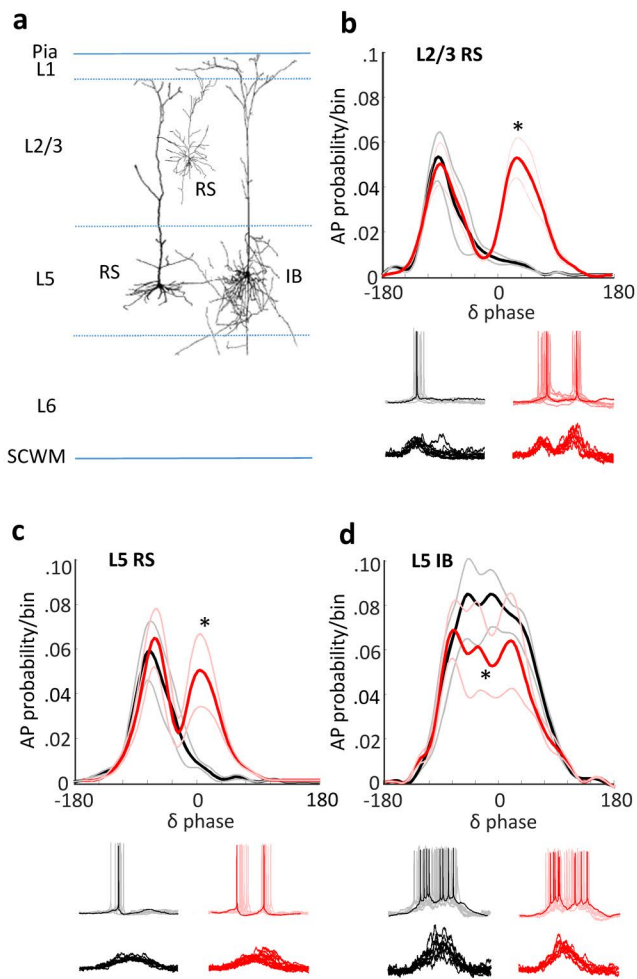


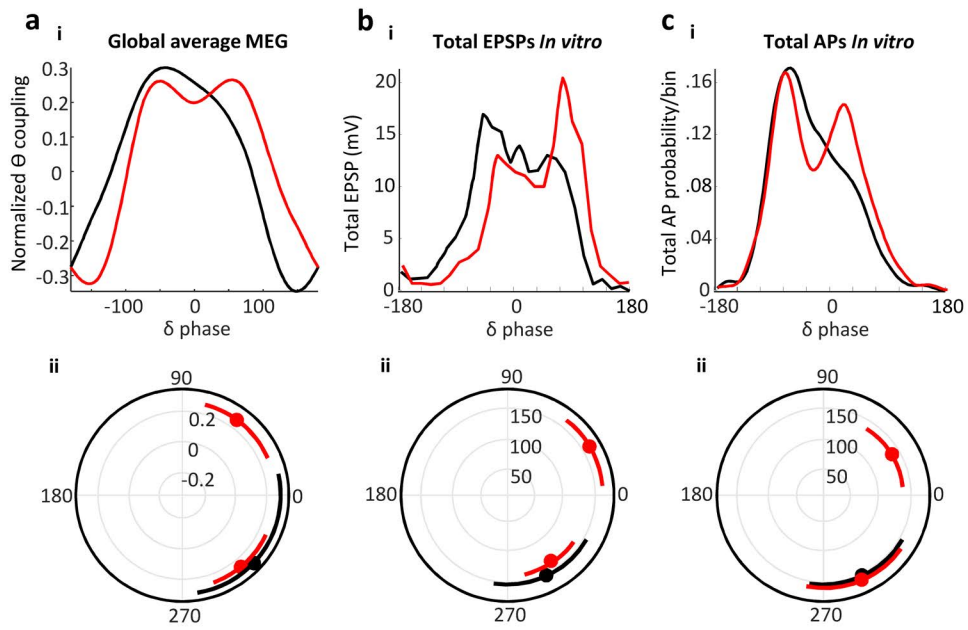




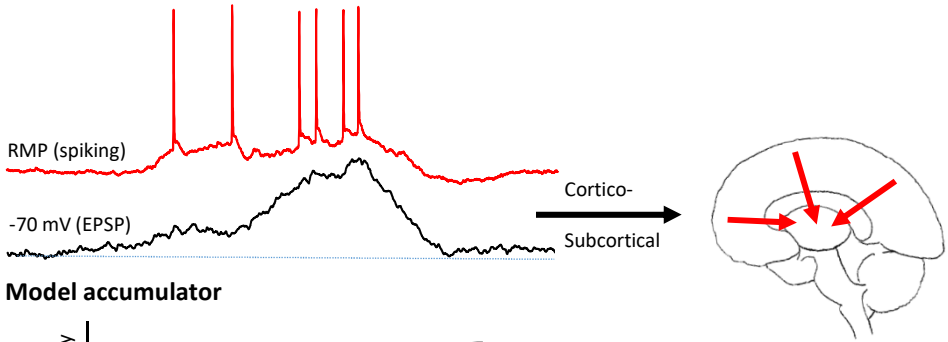




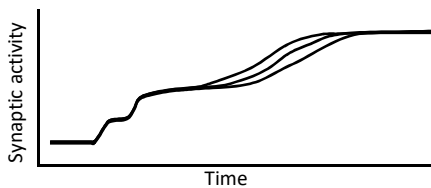




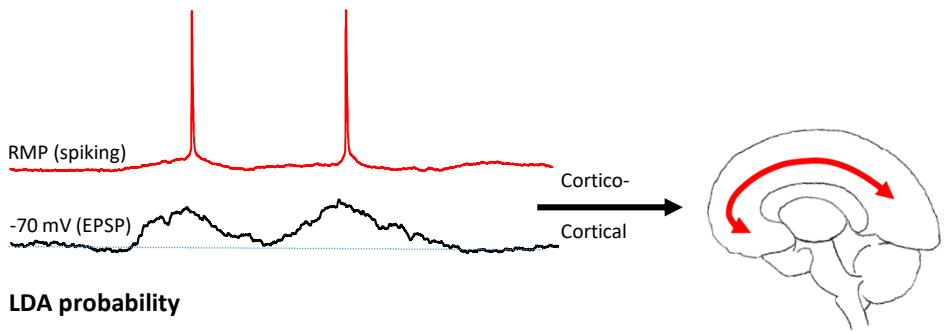
Accumulator-like neuron



Model accumulator



State-like neuron



LDA probability

